

# Collective Molecular Mechanisms in the $\text{CH}_3\text{NH}_3\text{PbI}_3$ Dissolution by Liquid Water

Claudia Caddeo,<sup>\*,†</sup> Maria Ilenia Saba,<sup>†</sup> Simone Meloni,<sup>‡</sup> Alessio Filippetti,<sup>†,¶</sup> and Alessandro Mattoni<sup>\*,†</sup>

<sup>†</sup> *Istituto Officina dei Materiali (CNR - IOM) Cagliari, Cittadella Universitaria, I-09042 Monserrato (Ca), Italy*

<sup>‡</sup> *Dept. of Mechanical and Aerospace Engineering, Università La Sapienza, via Eudossiana 18, 00184, Roma, Italy*

<sup>¶</sup> *Dipartimento di Fisica, Università degli Studi di Cagliari, Cittadella Universitaria, I-09042 Monserrato (Ca), Italy*

E-mail: caddeo@iom.cnr.it; mattoni@iom.cnr.it

## Abstract

The origin of the dissolution of MAPI crystals in liquid water is clarified by finite temperature molecular dynamics. It is found a thermally activated process with an energy barrier of 0.36 eV consisting of a layer by layer degradation with generation of inorganic  $\text{PbI}_2$  films and solvation of MA and I ions. We rationalize the effect of water on MAPI by identifying a transition from a reversible absorption and diffusion in presence of vapor, to the irreversible destruction of the crystal lattice in liquid due to a cooperative action of water molecules.

## Abbreviations

MAPbI<sub>3</sub>, MPMD

## Keywords

Perovskites

## Introduction

The importance of hybrid organic-inorganic perovskites has greatly increased in recent

years due to the exceptional photovoltaic properties of methylammonium lead trihalide  $\text{CH}_3\text{NH}_3\text{PbI}_3$  (MAPI) that make it a great promise for low cost, solution processable hybrid solar cells. This material with perovskite crystalline structure<sup>1</sup> has light absorption and charge transport properties comparable to those of the most efficient inorganic semiconductors<sup>2-4</sup> making it possible to manufacture 22% efficient MAPI solar cells<sup>5-7</sup>. The importance of MAPI extends far beyond photovoltaics with many possible applications ranging from optoelectronics<sup>8,9</sup> and lasing,<sup>10,11</sup> to photocatalysis<sup>12</sup> and thermoelectricity.<sup>13</sup>

Despite its excellent optoelectronic properties, MAPI has drawbacks such as e.g. the thermal instability at relatively low temperatures.<sup>14-16</sup> More importantly the material easily degrades in presence of highly polar solvents, like water.<sup>17</sup> Since solar cells operate at ambient conditions, the presence of water in air can easily induce the degradation of MAPI devices, also raising concerns on the dispersion of toxic lead in the environment.

Although it is in principle possible to protect the active layer by encapsulation,<sup>18-26</sup> waterproofing the material,<sup>27-30</sup> and to improve the stability by mixed-cations systems<sup>31</sup> a conclusive solution to the problem has not been

achieved so far. The understanding of the water-MAPI interaction and of the irreversible degradation mechanisms of hybrid perovskites is accordingly a key issue towards the development of usable devices.

Several experimental works have reported the effects of the exposure of MAPI to humidity: for example, Leguy *et al.*<sup>32</sup> have observed that when MAPI single crystals and thin films are exposed to water vapor at room temperature, hydrated crystal phases are formed. Notably such transformation can be reversed upon drying. Water absorption under vapor exposure is not well understood. Müller *et al.*<sup>33</sup> have observed water penetration into MAPI thin films within seconds at low 10% humidity, while Zhu *et al.*<sup>34</sup> did not observe infiltration up to 80% relative humidity. Most works agree that water infiltration is surface-originating, and defects or grain boundaries can enhance the process. Despite the different results, all experiments indicate that MAPI transformations under vapor conditions have a reversible character.

The exposure to liquid water instead gives always rise to irreversible dissolution of MAPI with the formation of  $\text{PbI}_2$ . Degradation is very effective in this conditions and it is observed already for very small amounts of liquid, like condensed drops on a thin film surface, or for fast dipping in water<sup>32,35</sup>. Degradation has been proposed to proceed through the loss of  $\text{CH}_3\text{NH}_3^+$  (with  $\text{I}^-$  as the counterion) and the consequent formation of the irreversible reaction product  $\text{PbI}_2$ .

Water has also an effect on the thermal degradation of MAPI at high temperature. In presence of humid air the kinetics is faster and characterized by a lower activation energy (0.96 eV in air versus 1.54 eV in vacuo).<sup>36</sup>

The molecular origin of dissolution has been searched by *ab initio* atomistic simulations. The studies of water on MAPI surfaces have been performed considering the two possible cases: MAI- or  $\text{PbI}_2$ -terminated surfaces. In the former case, i.e. the less stable MAI surface, it has been demonstrated that vapor and liquid water infiltration<sup>37-40</sup> are highly favored. Furthermore, **by using Car-Parrinello molecular dynamics (CPMD)**,<sup>41</sup> Mosconi *et al.*<sup>39</sup>

observed the solvation of a MAI unit detached from this surface in liquid water.

Conversely, the interaction of water with the  $\text{PbI}_2$ -terminated surface has slower dynamics far from reach for *ab initio*. In fact the full degradation of the  $\text{PbI}_2$ -terminated surface of MAPI<sup>39</sup> has never been observed, even in presence of liquid water. The computational cost of **CPMD** limits the the time scale to few tens of picoseconds, that is in any case too short to observe degradation of the  $\text{PbI}_2$ -terminated MAPI surface and to clarify the infiltration mechanism under controlled thermodynamic conditions. Accordingly, the molecular origin and the critical conditions for the overall MAPI dissolution in liquid water is still unexplored and requires alternative approaches.

Recently, a few model potentials have been reported for the study of MAPI over longer time and length scales by classical molecular dynamics.<sup>42-44</sup> In particular, the MYP potential<sup>42</sup> has demonstrated to reproduce several relevant properties of MAPI, such as orthorhombic-to-tetragonal transition, vibrational properties,<sup>45</sup> defects diffusion,<sup>46</sup> thermal transport properties<sup>47,48</sup> and the coexistence of ordered and disordered molecular domains in MAPI under specific thermal treatments.<sup>49</sup> To date, the only study of water/MAPI systems by model potential molecular dynamics (MPMD) has been performed by Gutierrez-Sevillano *et al.*<sup>50-52</sup> In their paper the Authors have adopted a force field that describes the MAPI precursors in solvent but that is not able to reproduce the properties of crystalline phase of MAPI. Here we want to simulate the dissolution process that, according to literature, involves the formation of  $\text{PbI}_2$  in liquid water; thus we need a force field able to model both the crystal and its dissolved components.

In this work we refine and extend the MYP force field to treat MAPI-water interactions and we study for the first time the full process of dissolution of MAPI crystal in water by finite temperature molecular dynamics. We are able to clarify the transition from reversible phenomena (such as vapor infiltration) to dissolution in liquid water. The kinetics reveals an Arrhenius behavior with activation energy

of 0.36 eV. Such an activation energy derives from a collective mechanism involving clusters of water molecules inducing the dissolution into ionic components. This decomposition process is fast and efficient in water and it represents a first step towards a slower irreversible degradation involving higher energy reactions  $\sim 1$  eV<sup>36,53</sup> such as deprotonation of methylammonium into methylamine<sup>36</sup> or methylammonium fragmentation into ammonia and CH<sub>3</sub>I.<sup>53,54</sup>

## Results and discussion

### System under Study

The typical system studied in this work consists of water molecules (either a single molecule, a cluster or a liquid layer) on top of a (001) PbI<sub>2</sub>-terminated MAPI slab (see Fig. 1). The choice of this surface stems from the fact that the (001) is one of the lowest energy cuts for MAPI.<sup>55</sup> Furthermore, the PbI<sub>2</sub> termination is interesting for applications since its surface states can act as intermediate levels for hole transfer.<sup>56</sup> **Additional calculations for the MAI-terminated surface were performed to validate results on degradation (see Supporting Information).**

The MAPI crystal is periodically replicated in the x-y directions and the lateral sizes are  $L_x=3.6$  nm x  $L_y=3.4$  nm. The slab is 1.8 nm thick along the z direction. For the study of vapor only one water molecule is put on the MAPI surface, corresponding to a surface density of  $2.4 \cdot 10^{-10}$  g/cm<sup>2</sup>, while for the liquid case, a 2.5-nm thick layer of water molecules is relaxed on top of the surface (surface density of  $\sim 8 \cdot 10^{-8}$  g/cm<sup>2</sup>). Overall up to  $10^4$  atoms were used in the simulations.

MAPI interatomic forces are described by a refined version of the MYP0 model potential<sup>57</sup> (referred to as MYP1). The main difference is a reduction of the Pb and I charges and the use of PbI Buckingham parameters close to the potential of Winkler et al<sup>58</sup> as interestingly suggested by Handley et al.<sup>59</sup> With respect to the Handley potential, the MYP1 is still able to re-

produce the orthorhombic-to-tetragonal transition. **An extensive validation of the model against DFT and experimental data can be found in the Supporting Information.**

The TIP3P model<sup>60</sup> is used for water. **This is a simple and widely adopted model for water with a low computational cost.** The MAPI-water interactions **are** described as the sum of Coulomb and Lennard-Jones (12-6) contributions and **are fitted on *ab initio* results for structure and energetics of suitable water-MAPI systems (see Supporting Information).** **In addition present model is able to reproduce the water/MAPI radial pair distribution functions (see Fig. 1), the easiness of water penetration inside the MAPI surface, and the experimentally observed insolubility of PbI<sub>2</sub> in water<sup>32,33</sup> (See Supporting Information).**

### Vapor phase analysis

First, we want to quantify the absorption of water on MAPI surface and its ability to infiltrate inside the MAPI crystal. Near saturation, a parcel of air contains  $\sim 28$  grams of water per cubic meter at room temperature and pressure, which corresponds to one water molecule per  $10^3$  nm<sup>3</sup>. With reference to our model, vapor phase conditions are thus attained by placing a single water molecule on the surface.

A single water put in front of the surface is attracted by the crystal and its oxygen eventually binds to a Pb atom of the surface giving rise to a polar Pb-O link of length  $\sim 2.8$  Å. This is in full agreement with DFT calculations. The averaged adhesion energy at room temperature of the water molecule on the surface is -0.41 eV. Once the molecule is anchored in this way it does not diffuse sizably at room temperature on the nanosecond time scale.

To study water infiltration within the MAPI crystal we calculated the associated energy gain of placing the water molecule inside the MAPI bulk,  $\Delta E_{in}$ . We find  $\Delta E_{in} = -0.29$  eV at room temperature, meaning that water infiltration is possible, though less convenient than water absorption on surface. Infiltration on a perfect crystal surface is found to be a rare event on the

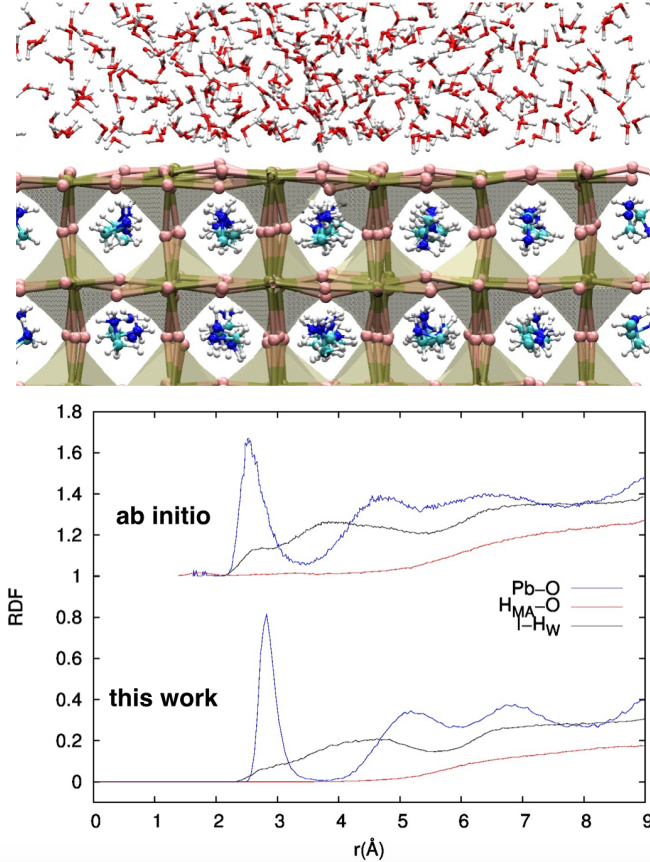


Figure 1: Top: snapshot of the simulated interface between the PbI<sub>2</sub>-terminated perovskite slab and the water layer. Red is O, white is H, pink is I, dark gold is Pb, cyan is C and blue is N. Polyhedra are made by triangles that connect all triplets of groups of atoms within a 4 Å radius. Bottom: I-H<sub>W</sub> (black), H<sub>MA</sub>-O (red), and Pb-O (blue) radial distribution functions (RDFs) at the interface, averaged over the first 25 ps. The top curves are shifted to enhance visibility and correspond to the *ab initio* RDFs of Ref. 39

nanosecond time scale indicating the existence of an energy barrier. This is consistent with the results of Koocher *et al.*<sup>38</sup> obtained by *ab initio* calculations reporting a static barrier between 0.023 and 0.23 eV, depending on the orientation of the MA cations. This is also consistent with results based on **CPMD simulations** of vapor<sup>61</sup>. In the case of damaged surfaces or in presence of more than one water molecule (see below), the infiltration process can be faster. Once infiltrated the molecule spends most of the time vibrating inside the MAPI tetragonal cell containing it. In agreement with Ref. 39, it is preferentially located on the sides of the perovskite cage, where it can form hydrogen bonds with the I atoms. The distribution of positions of hydrogen and oxygen atoms shows that H spends most of the time in proximity to I atoms, while O stays closer to the positive MA cation, as expected for electrostatic arguments (see e.g. top panel of Fig. 2), due to a tendency to form O-H links (see results at T=0K, Supporting Information).

Diffusion between adjacent cells is observed during long dynamics at room temperature. The molecule can jump from one PbI cage to the neighboring ones of the bulk. As temperature is raised, the water diffusion increases rapidly indicating a thermally activated process. An example of diffusion trajectory is reported in Fig.2. By fitting the average mean square displacements (MSD) with the Einstein relation  $MSD=6Dt$  we estimated the diffusion coefficients  $D$  at different temperatures. At T=300K a value of  $D=1.7 \cdot 10^{-8}$  cm<sup>2</sup>/s and an activation energy of 0.28 eV are found. Interestingly, this value is comparable with the case of water diffusion in perovskite oxides.<sup>62</sup>

## Liquid phase analysis

We focus now our attention on the opposite limit, i.e. MAPI surface in presence of liquid water (see Fig. 1). It is interesting first to calculate the adhesion energy  $\Delta E_{wet}$  necessary to separate a unit surface of water (wetting layer) from the crystal. An energy of -1.45 eV/nm<sup>2</sup> is found, corresponding to 0.23 N/m. As a term of comparison, the interaction energy between



Table 1: Energetics: energy gain ( $\Delta E$ ) for adhesion, infiltration and wetting. Kinetics: first two columns report the diffusion coefficient in the crystal ( $D$ ) at  $T=300$  K. Last two columns report the activation energy ( $E_A$ ) for diffusion and degradation.

Energetics			
		$\Delta E$	
adhesion		-0.41 eV	
infiltration		-0.29 eV	
wetting		1.45 eV/nm <sup>2</sup>	
Kinetics			
( T=300K)		$E_A$ (eV)	
$D$	$1.7 \cdot 10^{-8}$ cm <sup>2</sup> /s	diffusion	0.28
		degradation	0.36

water and silica is  $\sim 0.2$  N/m.<sup>63</sup> A summary of the water/MAPI energetics is reported in Table 1.

The wettability of the perovskites favors the contact between the water and the surface making it possible the degradation process. Accurate measurements of degradation velocity are not reported in literature but available data at room temperature indicate that a fast phenomenon with samples of thickness 1-100  $\mu\text{m}$  degraded in a few seconds.<sup>35</sup> In terms of microscopic quantities this corresponds to a few monolayers ( $\sim 1\text{nm}$ ) dissolved in  $10^4$ - $10^6$  ns. Accordingly, within the time scale typical of molecular dynamics simulations (up to 100 ns in the present study) it is not expected a sizable degradation at room temperature. This is in fact the case. However, as the temperature increases, the degradation kinetics rapidly increases. Already at 340 K, degradation events can be observed within the 100 ns. At higher temperatures the full degradation of a 4 nm thick crystal was observed during the dynamics. Under the hypothesis that the degradation velocity  $v$  follows an Arrhenius dependence on temperature ( $v \sim \exp(-E_A/K_B T)$ ), we plot  $\ln(v/l_0)$  vs  $1000/T$ , where  $l_0$  is the thickness of MAPI monolayer (0.63 nm) and  $t_0 = l_0/v$  is the time at which the first layer is completely degraded into  $\text{PbI}_2$ . The corresponding plot is reported in the bottom panel of Fig.3, and it

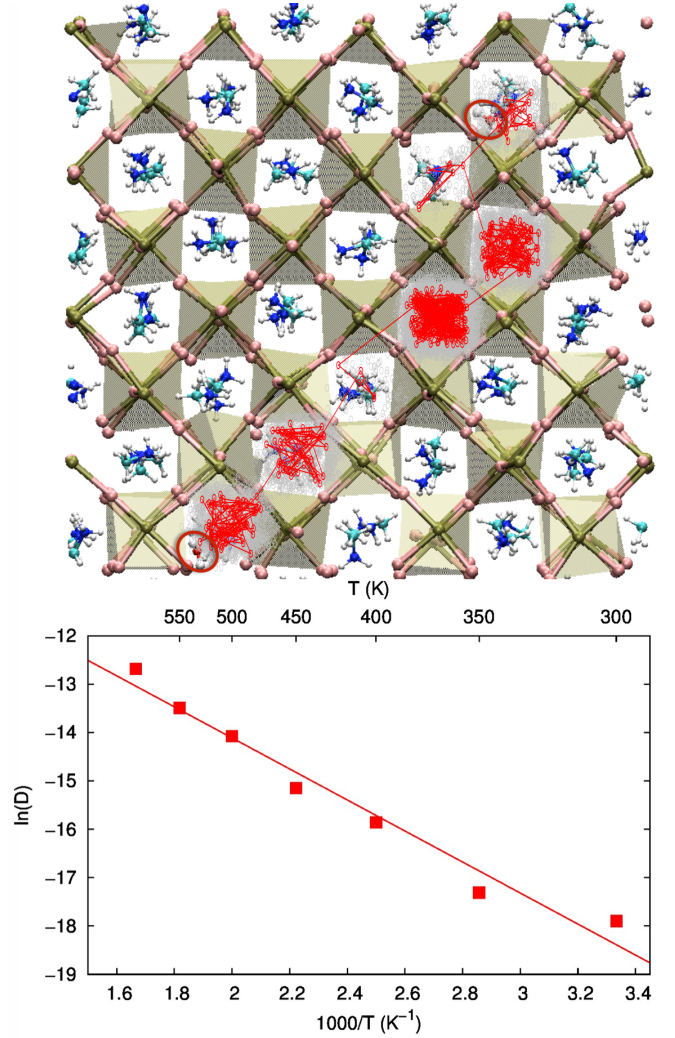


Figure 2: Top: illustration of the  $\text{H}_2\text{O}$  diffusion inside a MAPI bulk at  $T=550\text{K}$  during 5 ns. The water molecule jumps from a MAPI cell to an adjacent one in discrete steps. Red (grey) circles represent consecutive positions of oxygen (hydrogen) atoms of water along the trajectory. The initial and final position of the water molecule is also shown. Bottom: Arrhenius plot of the diffusion coefficients.

provides  $E_A = 0.36$  eV. Fig. 3 shows some snapshots of the degradation process simulated at  $T=480$  K: after 4 ns, the first layer has been transformed into  $\text{PbI}_2$  by the water, and it takes about 50 ns to degrade the whole slab. The degradation starts locally at some random point of the surface where a Pb-I bond breaks. After that the degradation tends to propagate laterally along the outmost layer of the crystal, and the MAPI is degraded in a layer-by-layer fashion.  $\text{PbI}_2$  layers are formed, while MAI is dis-

solved in water as  $\text{MA}^+$  molecules and  $\text{I}^-$  ions. This is in agreement with experimental results reporting  $\text{PbI}_2$  as product of degradation.<sup>35</sup>

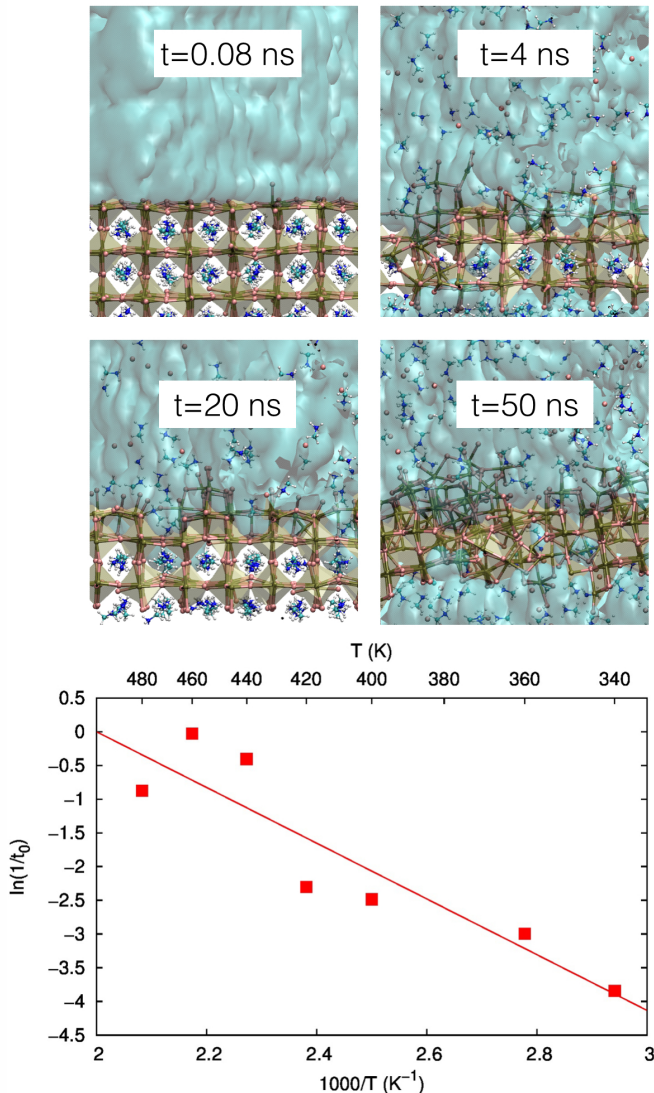


Figure 3: Top: snapshots of water degradation by liquid water at  $T=480\text{K}$ . Bottom: Arrhenius plot for MAPI degradation in liquid water.  $t_0 = l_0/v$  is the time (in nanoseconds) at which the first layer is completely transformed into  $\text{PbI}_2$ .

We have also performed the study of MAPI degradation by starting from the MAI terminated surface. To limit the computational cost we have considered only 300K and 480K. In agreement with the CPMD<sup>39</sup> (reporting the solvation of one MAI unit at room temperature in 8.5 ps) we observe a fast dissolution (within 10 ps) of outmost MAI layers (see Figure S4 of Supporting Information). After the

removal of external MAI units the surface evolves into a  $\text{PbI}_2$  terminated one. The surface is not perfectly flat due to the presence of an almost half coverage of I adatoms. At longer simulation time, we observe that the degradation is analogous to the  $\text{PbI}_2$  case. Eventually (at 480K and after 40ns annealing) the MAPI is fully dissolved into insoluble  $\text{PbI}_2$  and solvated MA and I ions (see Figure S5 of Supporting Information).

Past literature has indicated that an important channel for degradation of MAPI either under thermal stress or in presence of water is the deprotonation of methylammonium. In this case a dependence on the pH of water is expected, but the effect has been found to be modest.<sup>35</sup> Furthermore, the energy cost for deprotonation is high ( $\sim 1\text{eV}$ ). In the present study we find a lower activation energy mechanism for the spontaneous dissolution of the crystal into its ionic components in water. This fast process can possibly facilitate further decomposition by higher energy and slower fragmentation of methylammonium. As explained below the dissolution process relies on the ability of water molecules to damage the crystal by a collective action.

## Degradation and water coverage

Summarizing the previous results, we have found that the infiltration and diffusion of a single water molecule in MAPI crystal is possible and it does not induce degradation. Conversely, water in liquid phase is able to irreversibly dissolve the perovskite. It is natural to ask what is the reason for such a different behavior and whether it exists a minimal amount of water that is necessary and sufficient to degrade MAPI. In order to answer to this question we consider increasing amounts of water on MAPI surface and we study the damage induced on the surface as a function of the number of water molecules on the perovskite surface. We focus on  $T=340\text{K}$  as a similar analysis at room temperature, though possible, would require much longer simulations and a huge computational cost. We start by covering 10% of MAPI sur-

face sites by water molecules, and we then increase the coverage up to 100% (i.e. a complete water monolayer). The first degradation event is observed for 75% water coverage, corresponding to a surface density of  $5.9 \cdot 10^{-9}$  g/cm<sup>2</sup>: one I atom is lifted from the surface attracted by the surrounding H<sub>2</sub>O molecules (see Fig. 4a - 4b1). A Pb-I bond is thus broken, and two water molecules infiltrate inside the crystal (see Fig. 4b2- 4b3). A network of hydrogen bonds is formed between the water molecules and surface I atoms so as to bring the number of donor hydrogen bond per molecule toward its ideal value.<sup>64</sup> This is the first step of the water degradation, as detailed in previous section. It is interesting to compare the degradation energy calculated from the dynamics with the energy cost associated to the formation of I defects on the surface. In absence of water the formation energy is 0.62 eV. Notably, in presence of a cluster of four water molecules, this value lowers down to 0.26 eV close to the activation energy of 0.36 eV. This, together with the observation of the mechanism of water intrusion, suggest that the barrier is mainly due to the cost of forming the hydrated I defect. Furthermore, these results show that the presence of aggregated water molecules acts as catalyzer for the formation of such defects and the degradation of MAPI (see Supporting Information, Section S3).

For higher temperatures, this phenomenon is observed at lower water coverages: for example, at T=480 K a coverage as small as 20% is sufficient to initiate the surface degradation process. We remark here that the Pb-I bond breaking and subsequent multiple water infiltration is possible only when more than one H<sub>2</sub>O molecule is present in the proximity of the bond: in the simulated systems at low coverage, this correspond to having at least 3 water molecules around the I atom. These results clearly indicate a collective effect of water molecules.

In vapor phase (containing less than 1 molecule per 10<sup>3</sup>nm<sup>3</sup>) water is not able to damage the PbI network and we can speculate that water progressively infiltrates and diffuses as isolated molecules without damaging the crys-

tal until the formation of the hydrated phase. Conversely, when water is aggregated on the surface the irreversible degradation of the lattice can occur.

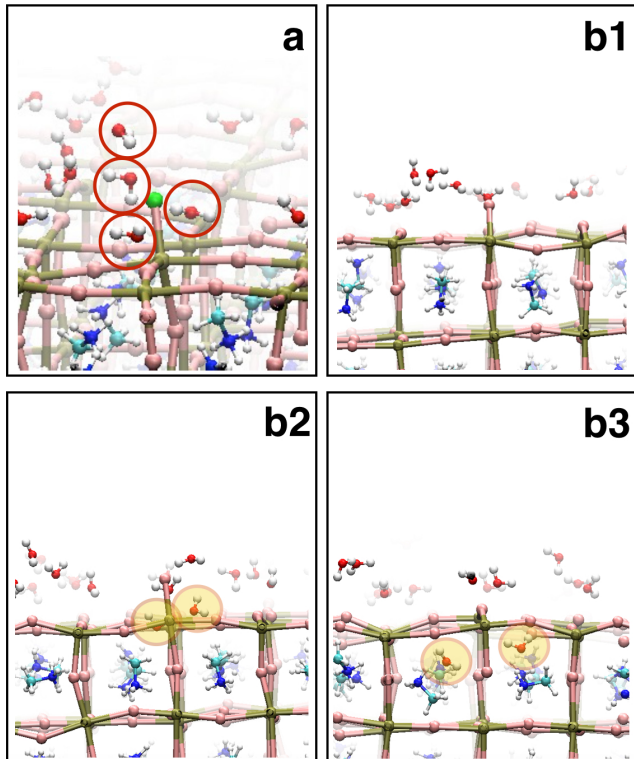


Figure 4: Snapshots taken during the simulation of 75% water coverage on MAPI surface at T=340 K. Panel a shows a view of three H<sub>2</sub>O molecules lifting a I atom (depicted in green for clarity). Panels b are subsequent moments of the simulation, showing water infiltration (the yellow circles indicate the infiltrated molecules).

## Conclusions

By calibrating a simple force-field for water/MAPI we have been able to study the interaction of MAPI crystal with vapor and to simulate its full dissolution in liquid water. The study provides a comprehensive picture of the transformation phenomena occurring in MAPI in presence of water. At room temperature the water vapor absorption is energetically favored by 0.07 eV and the infiltrated water molecules can diffuse without damaging the crystal structure, with a diffusion coefficient  $D=1.7 \cdot 10^{-8}$  cm<sup>2</sup>/s at room temperature.



On the contrary the dissolution of MAPI in liquid water is irreversible and thermally activated with a barrier of 0.36 eV. The underlying microscopic mechanism of degradation is explained as a collective action of water molecules that interacting with both Pb and I ions perturb the inorganic framework producing a water infiltration. In presence of bulk water, at the initial stages of the degradation, it is observed a tendency of liquid water to transform the material layer by layer, producing inorganic PbI<sub>2</sub> films and solvated MA and I ions.

By using models at increasing water coverage, we are able to rationalize the transition from the reversible kinetics in presence of water vapor to the irreversible degradation of the crystal in liquid. In particular, we show that three water molecules are needed to deteriorate locally the perfect PbI-terminated surface of the hybrid perovskite.

We point out that this is the first molecular dynamics simulation of MAPI dissolution by water which proceeds from the PbI<sub>2</sub>-terminated surface. Previous theoretical works on the picosecond scale were not able to observe PbI<sub>2</sub>-surface degradation and concluded that such a surface could act as a protective layer. Here, we show that on a longer nanosecond scale the MAPI degradation is indeed possible also from the PbI<sub>2</sub>-terminated surfaces, though it is less favored (i.e. slower) than from MAI-terminated ones. This study paves the way to further understanding of the role of extended defects and grain boundaries on the degradation in realistic samples.

## Computational details

Model potential molecular dynamics simulations were performed by using the LAMMPS code.<sup>65</sup> The long-range electrostatic forces were calculated by the particle-particle particle-mesh Ewald algorithm,<sup>66</sup> and van der Waals interactions were cutoff at 10 Å. The velocity-Verlet algorithm<sup>67</sup> with a time step as small as 0.5 fs was used to solve the equations of motion. Trajectories were analyzed by using the VMD 1.9 code.<sup>68</sup> After a conjugate gradient minimization

and a short (5 ps) low temperature (1K) relax, the systems were heated up to the temperatures of interest. Temperature was controlled by the Nose-Hoover thermostat.<sup>69,70</sup> Simulations in liquid water run for up to 50 ns. To estimate the diffusion coefficients for absorbed water molecules, we performed 10 independent simulations for each temperature and we averaged the molecule mean squared displacement (MSD).

**Acknowledgement** We acknowledge financial support by MIUR through Project PON NETERGIT and computational support from CINECA through ISCRA (projects THESTA, THEHYPE, MYPALLOY) and PRACE initiatives (project UNWRAP).

## References

1. Mattoni, A.; Filippetti, A.; Caddeo, C. Modeling hybrid perovskites by molecular dynamics. *J. Phys. Condens. Mat.* **2017**, *29*, 043001.
2. Mitzi, D. B. *Prog. Inorg. Chem.*; John Wiley and Sons, Inc., 2007; pp 1–121.
3. Stoumpos, C. C.; Malliakas, C. D.; Kanatzidis, M. G. Semiconducting Tin and Lead Iodide Perovskites with Organic Cations: Phase Transitions, High Mobilities, and Near-Infrared Photoluminescent Properties. *Inorg. Chem.* **2013**, *52*, 9019–9038.
4. Yin, W.-J.; Yang, J.-H.; Kang, J.; Yan, Y.; Wei, S.-H. Halide perovskite materials for solar cells: a theoretical review. *J. Mater. Chem. A* **2015**, *3*, 8926–8942.
5. Burschka, J.; Pellet, N.; Moon, S.-J.; Humphry-Baker, R.; Gao, P.; Nazeeruddin, M. K.; Gratzel, M. Sequential deposition as a route to high-performance perovskite-sensitized solar cells. *Nature* **2013**, *499*, 316–319.
6. Egger, D. A.; Rappe, A. M.; Kronik, L. Hybrid Organic-Inorganic Perovskites on the Move. *Acc. Chem. Res.* **2016**, *49*, 573–581.



7. Polman, A.; Knight, M.; Garnett, E. C.; Ehrler, B.; Sinke, W. C. Photovoltaic materials: Present efficiencies and future challenges. *Science* (80-. ). **2016**, *352*, aad4424–aad4424.
8. Ha, S. T.; Liu, X.; Zhang, Q.; Giovanni, D.; Sum, T. C.; Xiong, Q. Synthesis of Organic/Inorganic Lead Halide Perovskite Nanoplatelets: Towards High-Performance Perovskite Solar Cells and Optoelectronic Devices. *Adv. Opt. Mater.* **2014**, *2*, 838–844.
9. Yakunin, S.; Sytnyk, M.; Kriegner, D.; Shrestha, S.; Richter, M.; Matt, G. J.; Azimi, H.; Brabec, C. J.; Stangl, J.; Kovalenko, M. V. *et al.* Detection of X-ray photons by solution-processed lead halide perovskites. *Nat Photon* **2015**, *9*, 444–449.
10. Zhang, Q.; Ha, S. T.; Liu, X.; Sum, T. C.; Xiong, Q. Room-Temperature Near-Infrared High-Q Perovskite Whispering-Gallery Planar Nanolasers. *Nano Lett.* **2014**, *14*, 5995–6001.
11. Zhu, H.; Fu, Y.; Meng, F.; Wu, X.; Gong, Z.; Ding, Q.; Gustafsson, M. V.; Trinh, M. T.; Jin, S.; Zhu, X.-Y. Lead halide perovskite nanowire lasers with low lasing thresholds and high quality factors. *Nat Mater* **2015**, *14*, 636–642.
12. Park, S.; Chang, W. J.; Lee, C. W.; Park, S.; Ahn, H.-Y.; Nam, K. T. Photocatalytic hydrogen generation from hydriodic acid using methylammonium lead iodide in dynamic equilibrium with aqueous solution. *Nat. Energy* **2016**, *2*, 16185.
13. Filippetti, A.; Caddeo, C.; Delugas, P.; Mattoni, A. Appealing Perspectives of Hybrid Lead–Iodide Perovskites as Thermoelectric Materials. *J. Phys. Chem. C* **2016**, *120*, 28472–28479.
14. Dualeh, A.; Gao, P.; Seok, S. I.; Nazeeruddin, M. K.; Grätzel, M. Thermal Behavior of Methylammonium Lead-Trihalide Perovskite Photovoltaic Light Harvesters. *Chem. Mater.* **2014**, *26*, 6160–6164.
15. Eperon, G. E.; Stranks, S. D.; Menelaou, C.; Johnston, M. B.; Herz, L. M.; Snaith, H. J. Formamidinium lead trihalide: a broadly tunable perovskite for efficient planar heterojunction solar cells. *Energy Environ. Sci.* **2014**, *7*, 982–988.
16. Stranks, S. D.; Snaith, H. J. Metal-halide perovskites for photovoltaic and light-emitting devices. *Nat Nano* **2015**, *10*, 391–402.
17. Frost, J. M.; Butler, K. T.; Brivio, F.; Hendon, C. H.; van Schilfgaarde, M.; Walsh, A. Atomistic Origins of High-Performance in Hybrid Halide Perovskite Solar Cells. *Nano Letters* **2014**, *14*, 2584–2590.
18. Niu, G.; Li, W.; Meng, F.; Wang, L.; Dong, H.; Qiu, Y. Study on the stability of CH<sub>3</sub>NH<sub>3</sub>PbI<sub>3</sub> films and the effect of post-modification by aluminum oxide in all-solid-state hybrid solar cells. *J. Mater. Chem. A* **2014**, *2*, 705–710.
19. Yang, J.; Siempelkamp, B. D.; Liu, D.; Kelly, T. L. Investigation of CH<sub>3</sub>NH<sub>3</sub>PbI<sub>3</sub> Degradation Rates and Mechanisms in Controlled Humidity Environments Using in Situ Techniques. *ACS Nano* **2015**, *9*, 1955–1963.
20. Christians, J. A.; Herrera, P. A. M.; Kamat, P. V. Transformation of the Excited State and Photovoltaic Efficiency of CH<sub>3</sub>NH<sub>3</sub>PbI<sub>3</sub> Perovskite upon Controlled Exposure to Humidified Air. *J. Am. Chem. Soc.* **2015**, *137*, 1530–1538.
21. Han, Y.; Meyer, S.; Dkhissi, Y.; Weber, K.; Pringle, J. M.; Bach, U.; Spiccia, L.; Cheng, Y.-B. Degradation observations of encapsulated planar CH<sub>3</sub>NH<sub>3</sub>PbI<sub>3</sub> perovskite solar cells at high temperatures and humidity. *J. Mater. Chem. A* **2015**, *3*, 8139–8147.
22. Kang, S. M.; Ahn, N.; Lee, J.-W.; Choi, M.; Park, N.-G. Water-repellent perovskite solar cell. *J. Mater. Chem. A* **2014**, *2*, 20017–20021.

23. Jung, H. S.; Park, N.-G. Perovskite Solar Cells: From Materials to Devices. *Small* **2015**, *11*, 10–25.
24. Hwang, I.; Jeong, I.; Lee, J.; Ko, M. J.; Yong, K. Enhancing Stability of Perovskite Solar Cells to Moisture by the Facile Hydrophobic Passivation. *ACS Appl. Mater. Interfaces* **2015**, *7*, 17330–17336.
25. Eperon, G. E.; Burlakov, V. M.; Docampo, P.; Goriely, A.; Snaith, H. J. Morphological Control for High Performance, Solution-Processed Planar Heterojunction Perovskite Solar Cells. *Adv. Funct. Mater.* **2014**, *24*, 151–157.
26. Kim, I. S.; Cao, D. H.; Buchholz, D. B.; Emery, J. D.; Farha, O. K.; Hupp, J. T.; Kanatzidis, M. G.; Martinson, A. B. F. Liquid Water- and Heat-Resistant Hybrid Perovskite Photovoltaics via an Inverted ALD Oxide Electron Extraction Layer Design. *Nano Lett.* **2016**, *16*, 7786–7790.
27. Xie, F. X.; Zhang, D.; Su, H.; Ren, X.; Wong, K. S.; Grätzel, M.; Choy, W. C. H. Vacuum-Assisted Thermal Annealing of CH<sub>3</sub>NH<sub>3</sub>PbI<sub>3</sub> for Highly Stable and Efficient Perovskite Solar Cells. *ACS Nano* **2015**, *9*, 639–646.
28. Bass, K. K.; McAnally, R. E.; Zhou, S.; Djurovich, P. I.; Thompson, M. E.; Melot, B. C. Influence of moisture on the preparation, crystal structure, and photophysical properties of organohalide perovskites. *Chem. Commun.* **2014**, *50*, 15819–15822.
29. Zhou, H.; Chen, Q.; Li, G.; Luo, S.; Song, T.-b.; Duan, H.-S.; Hong, Z.; You, J.; Liu, Y.; Yang, Y. Interface engineering of highly efficient perovskite solar cells. *Science* **2014**, *345*, 542–546.
30. Li, B.; Fei, C.; Zheng, K.; Qu, X.; Pulverits, T.; Cao, G.; Tian, J. Constructing water-resistant CH<sub>3</sub>NH<sub>3</sub>PbI<sub>3</sub> perovskite films via coordination interaction. *J. Mater. Chem. A* **2016**, *4*, 17018–17024.
31. Saliba, M.; Matsui, T.; Domanski, K.; Seo, J.-Y.; Ummadisingu, A.; Zakeeruddin, S. M.; Correa-Baena, J.-P.; Tress, W. R.; Abate, A.; Hagfeldt, A. *et al.* Incorporation of rubidium cations into perovskite solar cells improves photovoltaic performance. *Science (80-. )*. **2016**, *354*, 206–209.
32. Leguy, A. M. A.; Hu, Y.; Campoy-Quiles, M.; Alonso, M. I.; Weber, O. J.; Azarhoosh, P.; van Schilfgaarde, M.; Weller, M. T.; Bein, T.; Nelson, J. *et al.* Reversible Hydration of CH<sub>3</sub>NH<sub>3</sub>PbI<sub>3</sub> in Films, Single Crystals, and Solar Cells. *Chem. Mater.* **2015**, *27*, 3397–3407.
33. Müller, C.; Glaser, T.; Plogmeyer, M.; Sendner, M.; Döring, S.; Bakulin, A. A.; Brzuska, C.; Scheer, R.; Pshenichnikov, M. S.; Kowalsky, W. *et al.* Water Infiltration in Methylammonium Lead Iodide Perovskite: Fast and Inconspicuous. *Chem. Mater.* **2015**, *27*, 7835–7841.
34. Zhu, Z.; Hadjiev, V. G.; Rong, Y.; Guo, R.; Cao, B.; Tang, Z.; Qin, F.; Li, Y.; Wang, Y.; Hao, F. *et al.* Interaction of Organic Cation with Water Molecule in Perovskite MAPbI<sub>3</sub>: From Dynamic Orientational Disorder to Hydrogen Bonding. *Chem. Mater.* **2016**, *28*, 7385–7393.
35. Hailegnaw, B.; Kirmayer, S.; Edri, E.; Hodes, G.; Cahen, D. Rain on Methylammonium Lead Iodide Based Perovskites: Possible Environmental Effects of Perovskite Solar Cells. *J. Phys. Chem. Lett.* **2015**, *6*, 1543–1547.
36. Smecca, E.; Numata, Y.; Deretzis, I.; Pellegrino, G.; Boninelli, S.; Miyasaka, T.; La Magna, A.; Alberti, A. Stability of solution-processed MAPbI<sub>3</sub> and FAPbI<sub>3</sub> layers. *Phys. Chem. Chem. Phys.* **2016**, *18*, 13413–13422.
37. Tong, C.-J.; Geng, W.; Tang, Z.-K.; Yam, C.-Y.; Fan, X.-L.; Liu, J.; Lau, W.-M.; Liu, L.-M. Uncovering the Veil of the Degradation in Perovskite CH<sub>3</sub>NH<sub>3</sub>PbI<sub>3</sub>

- upon Humidity Exposure: A First-Principles Study. *J. Phys. Chem. Lett.* **2015**, *6*, 3289–3295.
38. Koocher, N. Z.; Saldana-Greco, D.; Wang, F.; Liu, S.; Rappe, A. M. Polarization Dependence of Water Adsorption to CH<sub>3</sub>NH<sub>3</sub>PbI<sub>3</sub> (001) Surfaces. *J. Phys. Chem. Lett.* **2015**, *6*, 4371–4378.
  39. Mosconi, E.; Azpiroz, J. M.; De Angelis, F. Ab Initio Molecular Dynamics Simulations of Methylammonium Lead Iodide Perovskite Degradation by Water. *Chem. Mater.* **2015**, *27*, 4885–4892.
  40. Long, R.; Fang, W.; Prezhdo, O. V. Moderate Humidity Delays Electron-Hole Recombination in Hybrid Organic-Inorganic Perovskites: Time-Domain Ab Initio Simulations Rationalize Experiments. *J. Phys. Chem. Lett.* **2016**, *7*, 3215–3222.
  41. Car, R.; Parrinello, M. Unified Approach for Molecular Dynamics and Density-Functional Theory. *Phys. Rev. Lett.* **1985**, *55*, 2471–2474.
  42. Mattoni, A.; Filippetti, A.; Saba, M. I.; Delugas, P. Methylammonium Rotational Dynamics in Lead Halide Perovskite by Classical Molecular Dynamics: The Role of Temperature. *J. Phys. Chem. C* **2015**, *119*, 17421–17428.
  43. Hata, T.; Giorgi, G.; Yamashita, K. The Effects of the Organic-Inorganic Interactions on the Thermal Transport Properties of CH<sub>3</sub>NH<sub>3</sub>PbI<sub>3</sub>. *Nano Lett.* **2016**, *16*, 2749–2753.
  44. Qian, X.; Gu, X.; Yang, R. Lattice thermal conductivity of organic-inorganic hybrid perovskite CH<sub>3</sub>NH<sub>3</sub>PbI<sub>3</sub>. *Appl. Phys. Lett.* **2016**, *108*, 063902.
  45. Mattoni, A.; Filippetti, A.; Saba, M.; Caddeo, C.; Delugas, P. Temperature Evolution of Methylammonium Trihalide Vibrations at the Atomic Scale. *J. Phys. Chem. Lett.* **2016**, *7*, 529–535.
  46. Delugas, P.; Caddeo, C.; Filippetti, A.; Mattoni, A. Thermally Activated Point-Defects Diffusion in Methylammonium Lead Trihalide: Anisotropic and Ultra-High Mobility of Iodine. *J. Phys. Chem. Lett.* **2016**, *13*, 2356–2361.
  47. Caddeo, C.; Melis, C.; Saba, M. I.; Filippetti, A.; Colombo, L.; Mattoni, A. Tuning the thermal conductivity of methylammonium lead halide by the molecular substructure. *Phys. Chem. Chem. Phys.* **2016**, *18*, 24318–24324.
  48. Wang, M.; Lin, S. Anisotropic and Ultralow Phonon Thermal Transport in Organic-Inorganic Hybrid Perovskites: Atomistic Insights into Solar Cell Thermal Management and Thermoelectric Energy Conversion Efficiency. *Advanced Functional Materials* **2016**, *26*, 5297–5306.
  49. Dar, M. I.; Jacopin, G.; Meloni, S.; Mattoni, A.; Arora, N.; Boziki, A.; Zakeeruddin, S. M.; Rothlisberger, U.; Grätzel, M. Origin of unusual bandgap shift and dual emission in organic-inorganic lead halide perovskites. *Sci. Adv.* **2016**, *2*.
  50. Gutierrez-Sevillano, J. J.; Ahmad, S.; Calero, S.; Anta, J. A. Molecular dynamics simulations of organohalide perovskite precursors: solvent effects in the formation of perovskite solar cells. *Phys. Chem. Chem. Phys.* **2015**, *17*, 22770–22777.
  51. Horinek, D.; Mamatkulov, S. I.; Netz, R. R. Rational design of ion force fields based on thermodynamic solvation properties. *J. Chem. Phys.* **2009**, *130*, 124507.
  52. de Araujo, A. S.; Sonoda, M. T.; Piro, O. E.; ; Castellano, E. E. Development of New Cd<sup>2+</sup> and Pb<sup>2+</sup> Lennard-Jones Parameters for Liquid Simulations. *J. Phys. Chem. B* **2007**, *111*, 2219–2224.
  53. Delugas, P.; Filippetti, A.; Mattoni, A. Methylammonium fragmentation in amines as source of localized trap levels and the healing role of Cl in hybrid lead-iodide perovskites. *Phys. Rev. B* **2015**, *92*, 045301.

54. Juarez-Perez, E. J.; Hawash, Z.; Raga, S. R.; Ono, L. K.; Qi, Y. Thermal degradation of  $\text{CH}_3\text{NH}_3\text{PbI}_3$  perovskite into  $\text{NH}_3$  and  $\text{CH}_3\text{I}$  gases observed by coupled thermogravimetry-mass spectrometry analysis. *Energy Environ. Sci.* **2016**, *9*, 3406–3410.
55. Haruyama, J.; Sodeyama, K.; Han, L.; Tateyama, Y. Termination Dependence of Tetragonal  $\text{CH}_3\text{NH}_3\text{PbI}_3$  Surfaces for Perovskite Solar Cells. *J. Phys. Chem. Lett.* **2014**, *5*, 2903–2909.
56. Haruyama, J.; Sodeyama, K.; Han, L.; Tateyama, Y. Surface Properties of  $\text{CH}_3\text{NH}_3\text{PbI}_3$  for Perovskite Solar Cells. *Acc. Chem. Res.* **2016**, *49*, 554–561.
57. Mattoni, A.; Filippetti, A.; Saba, M. I.; Delugas, P. Methylammonium Rotational Dynamics in Lead Halide Perovskite by Classical Molecular Dynamics: The Role of Temperature. *J. Phys. Chem. C* **2015**, *119*, 17421–17428.
58. Winkler, B.; Dove, M. T.; Salje, E. K. H.; Leslie, M.; Palosz, B. Phonon stabilized polytypism in  $\text{PbI}_2$ : in situ Raman spectroscopy and transferable core-shell model calculations. *Journal of Physics: Condensed Matter* **1991**, *3*, 539–550.
59. Handley, C. M.; Freeman, C. L. A new potential for Methylammonium Lead Iodide. *Phys. Chem. Chem. Phys.* **2016**, *19*, 2313–2321.
60. Jorgensen, W. L.; Chandrasekhar, J.; Madura, J. D.; Impey, R. W.; Klein, M. L. Comparison of simple potential functions for simulating liquid water. *J. Chem. Phys.* **1983**, *79*, 926–935.
61. Zhang, L.; Ju, M.-G.; Liang, W. The effect of moisture on the structures and properties of lead halide perovskites: a first-principles theoretical investigation. *Phys. Chem. Chem. Phys.* **2016**, *18*, 23174–23183.
62. Animitsa, I.; Neiman, A.; Kochetova, N.; Korona, D.; Sharafutdinov, A. Chemical diffusion of water in the double perovskites  $\text{Ba}_4\text{Ca}_2\text{Nb}_2\text{O}_{11}$  and  $\text{Sr}_6\text{Ta}_2\text{O}_{11}$ . *Solid State Ionics* **2006**, *177*, 2363 – 2368, Solid State Ionics 15: Proceedings of the 15th International Conference on Solid State Ionics, Part {II}.
63. Lee, S. H.; Rossky, P. J. A comparison of the structure and dynamics of liquid water at hydrophobic and hydrophilic surfaces? a molecular dynamics simulation study. *J. Chem. Phys.* **1994**, *100*, 3334–3345.
64. Jorgensen, W. L.; Madura, J. D. Temperature and size dependence for Monte Carlo simulations of TIP4P water. *Mol. Phys.* **1985**, *56*, 1381–1392.
65. Plimpton, S. Fast Parallel Algorithms for Short-Range Molecular Dynamics. *J. Comp. Phys.* **1995**, *117*.
66. Swope, W. C.; Andersen, H. C.; Berens, P. H.; Wilson, K. R. A Computer Simulation Method for the Calculation of Equilibrium Constants for the Formation of Physical Clusters of Molecules: Application to Small Water Clusters. *J. Chem. Phys.* **1982**, *76*, 637–649.
67. Verlet, L. Computer Experiments on Classical Fluids. I. Thermodynamical Properties of Lennard-Jones Molecules. *Phys. Rev.* **1967**, *159*, 98–103.
68. Humphrey, W.; Dalke, A.; Schulten, K. VMD: Visual molecular dynamics. *J. Mol. Graphics* **1996**, *14*, 33 – 38.
69. Nosé, S. A Unified Formulation of the Constant Temperature Molecular Dynamics Methods. *J. Chem. Phys.* **1984**, *81*, 511–519.
70. Hoover, W. G. Canonical Dynamics: Equilibrium Phase-Space Distributions. *Phys. Rev. A* **1985**, *31*, 1695–1697.